molecular pharmaceutics

Article

pubs.acs.org/molecularpharmaceutics

Tracking Targeted Bimodal Nanovaccines: Immune Responses and Routing in Cells, Tissue, and Whole Organism

Luis J. Cruz,*[,†] Paul J. Tacken,[†] Ingrid S. Zeelenberg,[†] Mangala Srinivas,[†] Fernando Bonetto,[†] Bettina Weigelin,[‡] Christina Eich,[†] I. Jolanda de Vries,[†] and Carl G. Figdor*[,†]

[†]Department of Tumor Immunology, Radboud Institute for Molecular Life Sciences, Radboud University Medical Center, Nijmegen, The Netherlands

[‡]Department of Cell Biology, Radboud Institute for Molecular Life Sciences, Radboud University Medical Center, Nijmegen, The Netherlands

Supporting Information

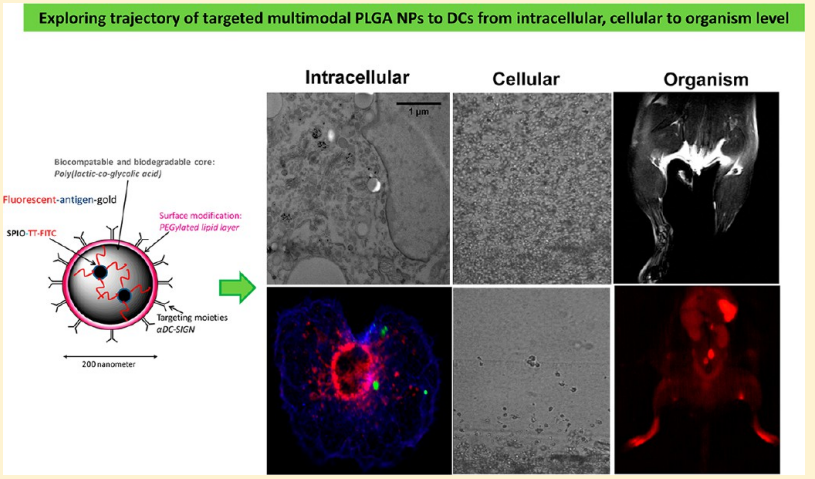

ABSTRACT: Dendritic cells (DCs) are the most potent antigen-presenting cells (APCs), involved in the induction of immunity and currently exploited for antitumor immunotherapies. An optimized noninvasive imaging modality capable of determining and quantifying DC-targeted nanoparticle (NP) trajectories could provide valuable information regarding therapeutic vaccine outcome. Here, targeted poly(D,L-lactide-*co*-glycolide) nanoparticles (PLGA NPs) recognizing DC receptors were equipped with superparamagnetic iron oxide particles (SPIO) or gold nanoparticles with fluorescently labeled antigen. The fluorescent label allowed for rapid analysis and quantification of DC-specific uptake of targeted PLGA NPs in comparison to uptake by other cells. Transmission electron microscopy (TEM) showed that a fraction of the encapsulated antigen reached the lysosomal compartment of DCs, where SPIO and gold were already partially released. However, part of the PLGA NPs localized within the cytoplasm, as confirmed by confocal microscopy. DCs targeted with NPs carrying SPIO or fluorescent antigen were detected within lymph nodes as early as 1 h after injection by magnetic resonance imaging (MRI). Despite the fact that targeting did not markedly affect PLGA NP biodistribution on organism and tissue level, it increased delivery of NPs to DCs residing in peripheral lymph nodes and resulted in enhanced T cell proliferation. In conclusion, two imaging agents within a single carrier allows tracking of targeted PLGA NPs at the subcellular, cellular, and organismal levels, thereby facilitating the rational design of in vivo targeted vaccination strategies.

KEYWORDS: *imaging, nanocarriers, biocompatible and biodegradable polymers, nanomaterials, contrast agents, fluorescence, magnetic resonance imaging, nanoparticles, dendritic cells*

1. INTRODUCTION

The successfulness of an immunotherapy inducing an antigen-specific immune response greatly depends on the efficient delivery of antigen and activation of antigen-presenting cells (APCs), such as dendritic cells (DCs). DCs are the most potent APCs, involved in the induction of adaptive immunity. In the peripheral tissues, DCs reside in an immature state until they encounter with pathogens. Ingestion of pathogens induces DC maturation and migration of DCs via the afferent lymphatics to the lymph nodes, where they present acquired antigens and activate specific T cells. To trigger an effective

Received: November 28, 2013
Revised: July 1, 2014
Accepted: October 7, 2014

immune response, efficient uptake of antigen by DCs in the peripheral tissues followed by migration to the regional lymph nodes is essential.[1]

Targeting DCs as a method of vaccination is a strategy that has gained increasing interest.[2,3] An ideal DC-targeting nanoparticle (NP) would harbor all of the following functionalities together: immunogenic antigen and adjuvant conjugation capabilities, targeted delivery system and biocompatibility, and no adverse effects on DC functions. Here, we describe the next generation of an NP that possesses most of these functionalities and is therefore ideal for in vivo cell tracking and imaging.

In recent years, NP/metal hybrid nanospheres have gained interest because of the synergetic combination of polymeric and metallic nanomaterials.[4] Among the metallic materials commonly exploited in the construction of nanoparticles/metal hybrid nanospheres, gold NPs and SPIO NPs are of particular interest due to their unique optical, magnetic, and electronic characteristics, as well as their excellent biocompatibility. It is expected that embedding gold and SPIO NPs into a nanosized polymer matrix, especially a biocompatible one such as PLGA, may not only provide the gold and SPIO nanoparticles with appropriate stabilization but also make it possible to design multifunctional nanomaterials for biomedical applications.

Alternatively, MRI is among the most widely applied noninvasive techniques used in clinical medicine for assessing anatomy and function of tissues. MRI offers several advantages such as excellent temporal and spatial resolution, no direct exposure to radioactive compounds, rapid in vivo acquisition of images, and a long effective imaging window. Iron based contrast agents such as SPIO, ultrasmall SPIO, and monocrystalline iron oxide nanoparticles typically produce contrast in the ^{1}H image by causing a localized drop in T_2*, creating a hypointense region in the surroundings of the contrast agent. Currently, a major drawback in the use of contrast agents for MRI is the lack of specific targeting signals, resulting in inefficient accumulation of contrast agents in target cells.

Despite the usefulness of MRI at the anatomical level, the sensitivity of MRI to monitor small tissue lesions, molecular activity, or cellular activities is much lower than that of fluorescence imaging, while fluorescence imaging is restricted by depth penetration limits. By integrating both MR and optical imaging techniques into one module, the limitations of each technique can be complemented by the other.[5−9]

Therefore, exploring multifunctional PLGA NPs should allow monitoring of NP biodistribution and localization of targeted DCs in the tissue and lymph nodes in real time visualization by both noninvasive MRI techniques and optical imaging. At the same time, internalization and antigen processing can be studied at the subcellular level in vitro by using both TEM (nanomaterial such as SPIO and gold NPs) and confocal microscopy imaging (fluorescent dyes).

In this study fluorescently labeled antigen conjugated to SPIO or gold NPs was encapsulated within a biocompatible polymer, PLGA. Moreover, antibodies recognizing human or mouse DC-specific receptors were coupled to the PLGA NP surface to ensure specific antigen delivery to DCs. We show that incorporation of fluorescently labeled antigen within PLGA NPs was useful to unravel intracellular routing by confocal/fluorescence microscopy and FACS analysis, while the inclusion of SPIO and gold NPs allowed tracking by TEM and MRI. Tissue biodistribution of targeted and nontargeted PLGA NPs was investigated by real time visualization using MRI and optical imaging. Next to determining subcellular, cellular, and tissue distribution of targeted nanovaccines, antigen uptake, degradation, and immunological outcome were assessed.

2. MATERIALS AND METHODS

2.1. Materials and Reagents. PLGA (Resomer RG 502 H, poly(D,L-lactide-*co*-glycolide) molar ratio 48:52 to 52:48) was purchased from Boehringer Ingelheim, Germany. Solvents for peptide synthesis and PLGA preparation (dichloromethane (DCM), *N*,*N*′-dimethylformamide (DMF), and ethyl acetate) were obtained from Sigma-Adrich (The Netherlands). Lipids purchased from Avanti Polar Lipids (USA) include 1,2-distearoyl-*sn*-glycero-3-phosphoethanolamine-*N*-[succinic acid-(polyethylene glycol)2000] (ammonium salt) and 1,2-distearoyl-*sn*-glycero-3-phosphoethanolamine-*N*-[methoxy-(polyethylene glycol)-2000] (ammonium salt) (mPEG 2000 PE). Iron(III) chloride hexahydrate ($FeCl_3 \cdot 6H_2O$) pure granulated, 99%, iron(II) chloride tetrahydrate ($FeCl_2 \cdot 4H_2O$) 99%, ammonium hydroxide (5 M), oleic acid, and PEG diamine were purchased from Fisher Scientific (USA) and Sigma-Adrich (The Netherlands) respectively.

The following Abs were used: anti-human HLA-DR/DP clone Q5/13[10] and Alexa Fluor 647-labeled goat anti-human and goat anti-mouse IgG (Invitrogen, The Netherlands); LAMP1-specific and the neck-specific αDC-SIGN Ab DCN46 and isotype-specific, AlexaFluor-conjugated secondary Abs. Besides, humanized αDC-SIGN (Ab hD1), its isotype control (h5G1.1), and mouse anti-human DC-SIGN Abs AZN-D1 (αDC-SIGN1) and AZN-D2 were described before[11,12] and were kindly provided by Alexion Pharmaceuticals (USA). Rat IgG F(ab′)2 fragment (Jackson ImmunoResearch) and F(ab′)2 fragments recognizing mouse DEC-205 were purified from NLDC-145 hybridoma.

2.2. Peptide Synthesis. The peptide antigen (FITC-**KK**QYIKANSKFIGITEL**KK**-COOH and FITC-**KK**QYIKANSKFIGITEL**KK**-Cys) with the extreme N-terminal modified with FITC were manually synthesized according to standard protocols of solid-phase peptide synthesis, using the 9-fluorenylmethoxycarbonyl (Fmoc)/*tert*-butyl strategy and CTC resin.[13]

2.3. Preparation of SPIO and Conjugation of Antigen to SPIO. SPIO were fabricated as described by Kumar et al.[14] FITC-TT-peptide, DQ-BSA, and Atto-647-OVA proteins were covalently attached to the SPIO using water-soluble carbodiimide. Unbound peptide and protein were removed by magnetic separation, and the FITC-TT-SPIO, DQ-BSA-SPIO, and Atto-647-OVA-SPIO were washed three times with PBS. The unbound FITC-TT peptide was measured by fluorescence relative to a standard curve using a CytoFluor II (Applied Biosystems, Foster City, CA) (Table 1), while the unbound DQ-BSA and Atto-647 OVA were quantified by Coomassie dye protein assay (Table 1).[15]

2.4. Preparation of Gold NPs and Conjugation of Antigens to Gold NPs. Gold NPs were produced as described by Cruz et al.[16] After that, the conjugation was performed in the presence of an excess of peptide and protein. FITC-TT peptide-Cys (1 mg solubilized in 1 mL of water) was added dropwise to a 10 mL solution of gold NPs at room temperature with magnetic stirring and agitation for 15 min. The gold NP-FITC-TT peptide complexes were then purified by dialysis (for 3 days in a membrane Spectra/MWCO: 6−8000) against

Table 1. Determination of Fluorescent Antigen Conjugated to SPIO and Gold NPs and Size Distribution[a]

samples	efficiency of fluorescent antigen conjugated to nanomaterials ± SD (%)	nanomaterial size ± SD (nm)	PDI
FITC-TT-SPIO	50.8 ± 5.3	8.2 ± 1.5	0.157
FITC-TT-gold NP	47.1 ± 2.1	8.6 ± 0.9	0.165
DQ-BSA-SPIO	19.4 ± 3.4	10.4 ± 2.1	0.188
DQ-BSA-gold NP	11.0 ± 1.3	11.2 ± 1.6	0.192
Atto-647-OVA-SPIO	12.0 ± 2.3	10.0 ± 1.8	0.197

[a]Determination of fluorescent antigen and size distribution of SPIO and gold NPs. Nanoparticle size data represent the mean value ± SD of dynamic light scattering data. Fluorescent antigen conjugated to SPIO or gold NPs was determined by measuring fluorescence relative to standard curves. The amount of DQ-BSA or Atto-647-OVA conjugated to SPIO or gold NPs was determined by Coomassie dye protein assay and is depicted as the mean ± SD of two experiments.

sodium citrate 2.2 mM, and the solution was changed two times per day. To determine the number of peptide molecules per gold NP, nondialyzed aliquots of the conjugated solutions (2.5 mL) were centrifuged at 14000 rpm for 10 min. The supernatant was lyophilized and then analyzed by RP-HPLC to determine the amount of unconjugated peptide. It was observed that 47 ± 2.1% (470 μg) of peptide was conjugated to the gold NPs (10 mL solution of gold NPs).

To bind DQ-BSA protein to gold NPs, the DQ-BSA protein (2 mg/mL in PBS) was conjugated with the heterobifunctional reagent SPDP (SPDP/DQ-BSA, 10/1 molar ratio). Excess SPDP was removed by a Sephadex G-50 spin column. As estimated spectrophotometrically, there were 3 PDP residues per DQ-BSA molecule. Thiolated DQ-BSA was obtained by reducing the DQ-BSA-PDP with DTT 50 mM at pH = 4.5. Excess DTT was removed using a Sephadex G-50 spin column. Activated DQ-BSA-SH was added dropwise to 10 mL of gold NP solution. The DQ-BSA-gold NP complexes were purified by centrifugation using Amicon 100 kDa (Centriplus, Millipore Corporation, U.S.A) to remove the excess of the DQ-BSA. The concentration of DQ-BSA per gold NP was determined by Coomassie dye protein assay. It was observed that 11 ± 1.3% (110 μg) of DQ-BSA was conjugated to the gold NP (Table 1).

2.5. PLGA NP Preparation. PLGA NPs with entrapped fluorescently labeled antigens conjugated to SPIO or gold nanospheres were prepared using an o/w emulsion and solvent evaporation−extraction method.[17] In brief, 90 mg of PLGA in 3 mL of DCM containing the FITC-TT-SPIO or FITC-TT-Gold or DQ-BSA-SPIO or DQ-BSA-gold or Atto-647-OVA-SPIO (30 mg) was added dropwise to 25 mL of aqueous 2% (w/v) PVA and emulsified for 90 s using a sonicator (Branson, sonofier 250). A combination of lipids (DSPE-PEG(2000)-succinic acid (8 mg) and mPEG 2000 PE (8 mg)) were dissolved in DCM and added to the vial. The DCM was removed by a stream of nitrogen gas. Subsequently, the emulsion was rapidly added to the vial containing the lipids and the solution was homogenized during 30 s. Following overnight evaporation of the solvent at 4 °C, the PLGA NPs were collected by ultracentrifugation at 60000*g* for 30 min, washed three times with distilled water, and lyophilized. PLGA NP-Abs was prepared as described by Cruz et al.[18] The amount of Abs on the particle surface was determined by Coomassie dye protein assay (Table 2).[15] PLGA NP physical properties were assessed by SEM, TEM, dynamic light scattering, and zeta-potential as reported previously.[18]

2.6. Determination of SPIO and Gold Contents Inside of PLGA NPs. Entrapment efficiency of fluorescently labeled antigen−nanosphere complexes within PLGA was determined by digesting 10 mg of NPs in 1 mL of 0.8 mol/L NaOH overnight at 37 °C. The FITC-peptide-gold NP, FITC-peptide-SPIO, DQ-BSA-gold, and DQ-BSA-SPIO were separated by centrifugation, washed several times, and weighed. Lyophilized samples of the preparation and the FITC-peptide-SPIO and FITC-peptide-gold NP were also measured by fluorescence

Table 2. Determination of Complex Fluorescent Antigen-SPIO or Gold within Targeted and Nontargeted PLGA, Size Distribution, and Zeta Potential[a]

samples	loading fluorescent antigen efficiency (%, w/w)	SPIO or gold NPs (μg/mg PLGA)	size ± SD (nm)	PDI ± SD	width	zeta potential ± SD (mV)	Abs (μg/mg PLGA)
NP(DQ-BSA-gold)	4.1 ± 1.2	272 ± 42	223.0 ± 9.2	0.189 ± 0.086	67.3	−33.8 ± 1.8	
NP(FITC-TT-gold)	41.9 ± 8.3	260 ± 37	219.0 ± 5.1	0.169 ± 0.087	71.1	−35.9 ± 1.6	
NP(FITC-TT-gold)-Isot	12.2 ± 6.3	260 ± 37	246.5 ± 8.0	0.176 ± 0.087	83.4	−16.9 ± 1.6	19.9 ± 2.2
NP(FITC-TT-gold)-αDC-SIGN	12.2 ± 6.3	260 ± 37	251.6 ± 10.9	0.161 ± 0.077	98.9	−15.7 ± 1.8	19.8 ± 1.7
NP(DQ-BSA-SPIO)	5.6 ± 1.4	290 ± 56	201.5 ± 7.9	0.146 ± 0.065	72.1	−36.1 ± 1.7	
NP(FITC-TT-SPIO)	16.3 ± 4.1	320 ± 60	199.4 ± 6.8	0.111 ± 0.045	56.9	−34.9 ± 3.6	
NP(FITC-TT-SPIO)-Isot	16.3 ± 4.1	320 ± 60	225.6 ± 12.6	0.117 ± 0.056	68.7	−14.5 ± 4.6	19.3 ± 1.8
NP(FITC-TT-SPIO)-αDC-SIGN	16.3 ± 4.1	320 ± 60	227.8 ± 11.2	0.197 ± 0.066	72.1	−12.7 ± 3.5	18.1 ± 1.5
NP-(Atto-647-OVA-SPIO)	14.0 ± 3.1	284 ± 42	210 ± 12.4	0.189 ± 0.086	79.2	−29.5 ± 1.8	
NP-(Atto-647-OVA-SPIO)-Isot	14.0 ± 3.1	284 ± 42	218.3 ± 16.4	0.220 ± 0.094	89.2	−11.3 ± 1.6	27.6 ± 2.1
NP-(Atto-647-OVA-SPIO)-αDEC-205	14.0 ± 3.1	284 ± 42	219.5 ± 14.1	0.212 ± 0.091	83.5	−13.2 ± 1.8	24.2 ± 2.4

[a]PLGA NPs were characterized by DLS measurements and zeta potential measurements. The amount of antigens encapsulated inside of PLGA NPs was determined by Coomassie dye protein assay. The amount of antibody introduced into the PLGA NPs was determined indirectly by Coomassie Plus Protein Assay Reagent by measuring a small aliquot from the antibody solution at the starting point and at the end of the reaction.

relative to a standard curve using a CytoFluor II (Applied Biosystems, Foster City, CA). The DQ-BSA-gold and DQ-BSA-SPIO were quantified by Coomassie protein assay (Table 2).

2.7. Characterization of SPIO and Gold within PLGA NPs by MRI. The presence of SPIO and gold inside PLGA NPs was assessed by MRI. A fixed amount (1 mg) of unlabeled and labeled PLGA NPs with gold and SPIO was embedded into 100 μL of agar gel to produce a homogeneous sample. Each sample was introduced into capillary tubes, and both tubes were inserted into a 2 mL Eppendorf tube previously filled with agar gel. The whole sample was imaged in a 7T Clinscan MRI scanner (Bruker Biospin MRI GmbH, Germany) with a proton birdcage volume coil. The sample was placed inside the coil, and a turbo spin echo pulse sequence (TE/TR = 7.7/900 ms, 0.12 × 0.12 × 1 mm resolution, turbo factor = 10) was used to obtain images.

2.8. Cells. Granulocytes and peripheral blood mononuclear cells (PBMCs) were obtained from buffy coats of healthy individuals and were purified using Ficoll density centrifugation.[11] Adherent monocytes were cultured in the presence of IL-4 and GM-CSF (500 and 800 U/mL, respectively; Schering-Plough International, USA) for 6 days to obtain immature DCs. DCs were cryopreserved until use. Cells were cultured in X-VIVO 15 medium (Cambrex, Belgium) supplemented with 2% human serum. Mouse bone marrow derived DCs (BMDCs) were obtained from C57Bl/6J femur and tibia and cultured in IMDM medium (Gibco, Invitrogen) containing 10% fetal calf serum and 30% GM-CSF-containing J558 conditioned medium, prepared as described before.[19] BMDCs were routinely checked for purity and maturation markers by flow cytometry. OT-1 $CD8^+$ T cells were isolated from lymph node and spleen suspensions of OT-1 mice. The OT-I cells were sorted using Myltenyi Biotec $CD8^+$ magnetic cell sorting kit. Phenotypic characterization of OT-I cells was performed using a CyAn flow cytometer (Beckman Coulter).

2.9. Localization of PLGA NP within DCs by TEM. The DCs were incubated with PLGA NP(FITC-TT-SPIO)-αDC-SIGN and PLGA NP(FITC-TT-gold)-αDC-SIGN for 24 h and fixated with 2% glutaraldehyde/0.1 mol/L sodium cacodylate buffer (pH 7.3). Then, the cells were rinsed in 0.1 mol/L sodium cacodylate buffer, postfixed in 1% OsO4/0.1 mol/L sodium cacodylate buffer, rinsed in 0.1 mol/L sodium cacodylate buffer, and spun down in 2% agar/0.1 mol/L sodium cacodylate buffer. The cell pellet was cut in small cubes, dehydrated through graded alcohol, and embedded in Agar 100 resin (Agar Scientific Limited, England). Ultrathin sections were cut on a Leica Reichert Ultracut S picked up on Formvar coated copper grids, contrasted with uranyl acetate and lead citrate and examined with a Jeol 1010 transmission electron microscope (Jeol, Akishima Tokyo, Japan). Images were taken on Imaging plates (Ditabis) or with a CCD Megaview III (SIS) camera (Münster, Germany).

2.10. Binding and Uptake of PLGA NP by DCs Using Confocal Microscopy. Binding and internalization of PLGA NPs was confirmed by confocal microscopy. Human monocyte-derived DCs were cultured on fibronectin-coated coverslips for 1 h in the presence of PLGA NP vaccines harboring FITC-TT peptide-gold Ag (green) that were coated with αDC-SIGN1. Subsequently, DCs were fixed, permeabilized, and stained with LAMP1-specific Ab (red) and the neck-specific αDC-SIGN Ab DCN46 (blue) and isotype-specific, AlexaFluor-conjugated secondary Abs. Subsequently, cells were analyzed using an Olympus FV1000 confocal laser scanning microscope. Images represent middle focal planes of DCs.

2.11. Iron Staining of SPIO within DCs and Tissue. Prussian blue staining was performed to detect SPIO within these cells and tissue.[18] The samples were viewed in a Leica DMLB microscope.

2.12. Binding and Uptake of PLGA NP by DCs Using Flow Cytometry. PLGA NP binding was studied by incubating cells with 20 μg/mL of NP(FITC-TT-SPIO)-αDC-SIGN, NP(FITC-TT-gold)-αDC-SIGN, NP(FITC-TT-gold)-isotype, NP(FITC-TT-gold)-isotype, or NPs without Abs for 1 h at 4 °C in culture medium. Subsequently, cells were washed and analyzed by flow cytometry. Uptake was studied by incubating cells with 20 μg/mL of the same PLGA NPs at 37 °C for 1 h. The cells were washed and analyzed by flow cytometry on a FacsCalibur (Becton Dickinson, USA). In part of the experiments a mixture of the anti-human DC-SIGN Abs AZN-D1 (50 μg/mL) and AZN-D2 (50 μg/mL) was added to the cells 30 min before addition of the PLGA NP carriers to preblock DC-SIGN. To determine the specificity by which the PLGA NPs target DCs, leukocytes were mixed with monocyte-derived DCs in a 20:1 ratio in culture medium. Cells were incubated with PLGA NP-αDC-SIGN, isotype, and PLGA NP without Abs (50 μg/mL) at 37 °C for 2 h. Cells were washed and stained with a mannose receptor-specific Ab (clone 19.2, Becton Dickinson) or isotype control Ab to specifically detect DCs. Subsequently, cells were analyzed by flow cytometry on a FacsCalibur. The cell associated fluorescence was calculated by dividing the mean cell fluorescence intensity (mfi) for a given sample by the mfi of DCs incubated with PLGA NP-αDC-SIGN, which was set at 100%.

2.13. T Cell Proliferation Assay Using Human Cells. Immature DCs (iDCs) and PBLs of donors that respond to TT-antigen were obtained from buffy coats after informed consent. DCs were incubated with PLGA NP(FITC-TT-SPIO)-αDC-SIGN and PLGA NP(FITC-TT-gold)-αDC-SIGN or similar NPs coated with isotype control Abs (containing 25 ng to 1 ng of FITC-TT peptide) for 2 days at 37 °C. Nontreated iDCs were taken along as negative control. Following washing, the TT-responsive PBLs were added to the iDCs (1:10 hDC/T cell relationship). Four days after addition of the PBLs, proliferative responses were determined by adding tritiated thymidine (1 μCi [0.037 MBq]/well; MP Biomedicals, Amsterdam, The Netherlands) to the cell cultures. Tritiated thymidine incorporation was measured after 16 h in a scintillation counter. The proliferation index per condition was calculated as mean counts per minute (cpm) of wells with antigen-loaded iDCs and PBLs divided by the mean cpm of control wells containing nontreated iDCs and PBLs non-stimulated wells.

2.14. T Cell Proliferation Assay Using Mouse Cells. Day 8 mouse BMDCs were cultured at 5000 cells/well with 50000 OT-1 cells/well and various amounts of targeted and nontargeted PLGA NPs carrying OVA. To test for T cell activation, culture supernatant was harvested after 3 days to determine IFN-γ production by ELISA (Thermo Scientific). To determine T cell proliferation, tritiated thymidine (1 μCi [0.037 MBq]/well; MP Biomedicals) was added to the cell cultures. Tritiated thymidine incorporation was measured after 16 h in a β-scintillation counter.

2.15. 3D Collagen Migration Assay. The assay was carried out as described.[20] Briefly, DC loading with distinct NP(FITC-TT-gold)-αDC-SIGN and NP(FITC-TT-SPIO)-

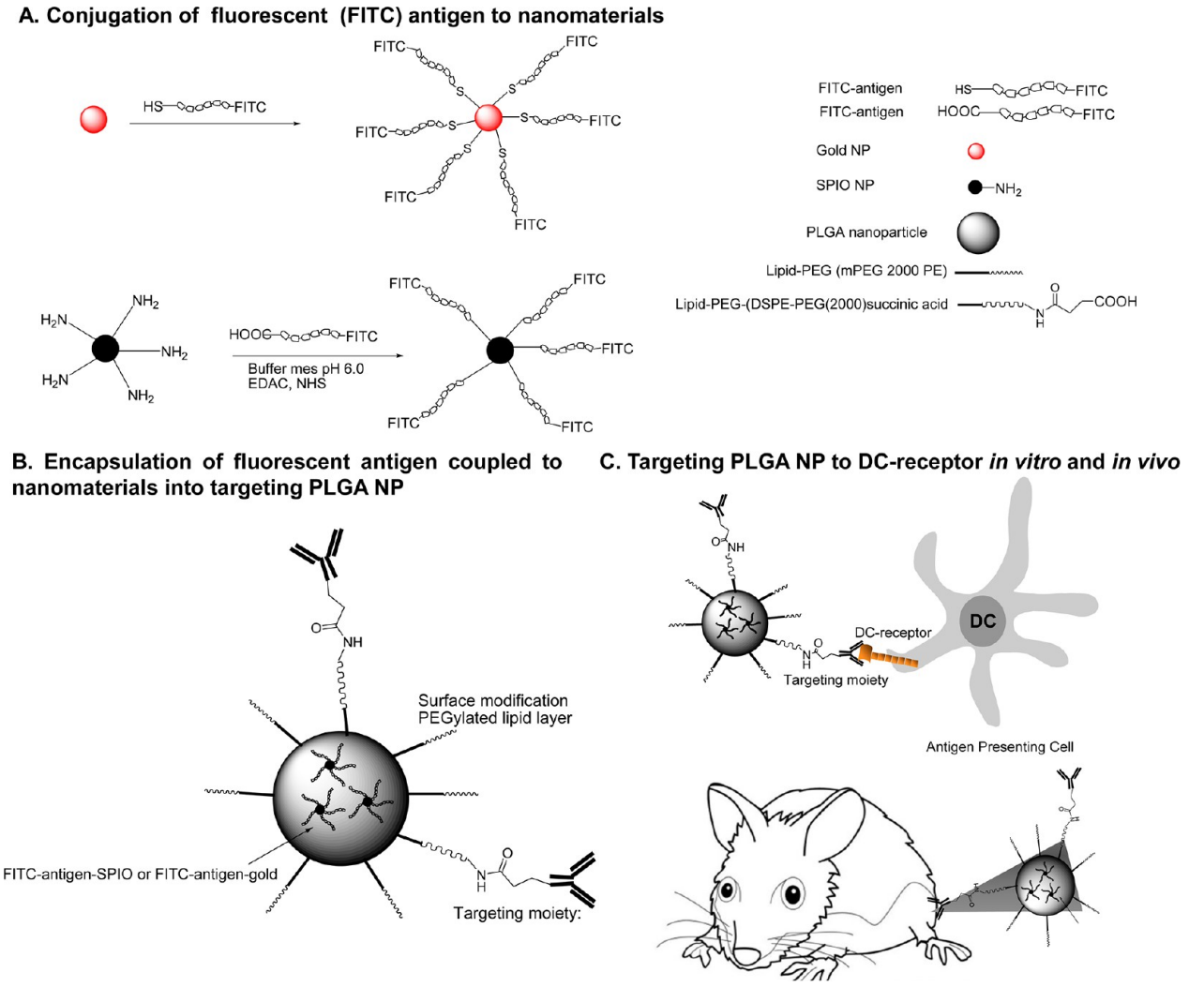

Figure 1. Schematic illustration of bimodal targeted NP carrier. NPs were generated containing SPIO or gold NPs, and fluorescently labeled antigen for flow cytometry and confocal imaging purposes. (A) Conjugation of fluorescent antigen to nanomaterials, SPIO or gold NPs. The fluorescent antigens were covalently bound to the SPIO nanoparticles via amide bond, while gold NPs and fluorescent antigens were covalently conjugated via thiol group. (B) Fluorescent antigen−nanomaterial complexes were encapsulated in a PLGA matrix. The PEG-lipid prevents nonspecific interactions, and the carboxyl functionalized PEG-lipid allows introduction of Abs on the PLGA surface for targeting purposes. (C) Tracking of targeted PLGA NPs to DC-receptors in human and mouse setting in vitro. Targeted-bimodal PLGA NPs can be tracked in human DC. Antigen content allows analysis of immune responses following targeted delivery of NPs.

αDC-SIGN were incorporated into a 3D collagen matrix (PureCol, Inamed BioMaterials, final concentration 1.7 mg/mL; 5×10^6 cells/mL) and overlaid with a cell-free second collagen matrix layer which contained CCL21 at low concentration (0.5 μg/mL).To establish a steeper chemokine gradient, medium containing a high concentration of chemokine (CCL21, 1 μg/mL) was added adjacent to the cell-free collagen compartment. DC migration into the cell-free collagen layer was recorded by digital time-lapse microscopy at a 2 min frame interval for up to 12 h. Computer-assisted cell tracking of randomly selected cells was performed as described.[21]

2.16. In Vivo Real Time Visualization and Biodistribution of PLGA NPs by Optical Imaging. Mice (C57Bl/6N, Charles River Wiga, Sutzfield, Germany) received a footpad injection with PLGA NPs containing Atto647-OVA-SPIO. Localization and biodistribution of targeted and nontargeted PLGA NPs were determined by fluorescence measurements using a FluorVivo (INDEC Biosystems).

2.17. In Vivo Real Time Visualization by MRI. MRI measurements were performed using a 7 T Bruker Ultra Shielded Refrigerated magnet (Bruker, Germany). Mice were anesthetized using isoflurane and placed in a homemade coil to detect the ^{1}H signal. During the measurements isoflurane flow was adapted to keep a constant low breathing rate. The body temperature of the mouse was regulated by warm air flow and kept at 37 °C. A turbo spin echo sequence with TR/TE 2000/31 ms was used to acquire the ^{1}H images. The voxel size was 0.159 × 0.159 × 1 mm.

2.18. Ex Vivo Analysis of Cellular Uptake of PLGA NPs within the Lymph Nodes. Mice (C57Bl/6N, Charles River Wiga, Sutzfield, Germany) received a footpad injection with targeted and nontargeted PLGA NPs containing Atto647-OVA-SPIO. Ex vivo PLGA NP uptake by cells was analyzed 24 h after injection by sacrificing the animals and isolating the popliteal and lumbar lymph nodes. Single cell suspensions were prepared to determine the mean fluorescence intensity of Atto647-OVA-SPIO in F4/80-CD11b+CD11c+ DC as a measure for PLGA

dx.doi.org/10.1021/mp400717r | Mol. Pharmaceutics XXXX, XXX, XXX−XXX

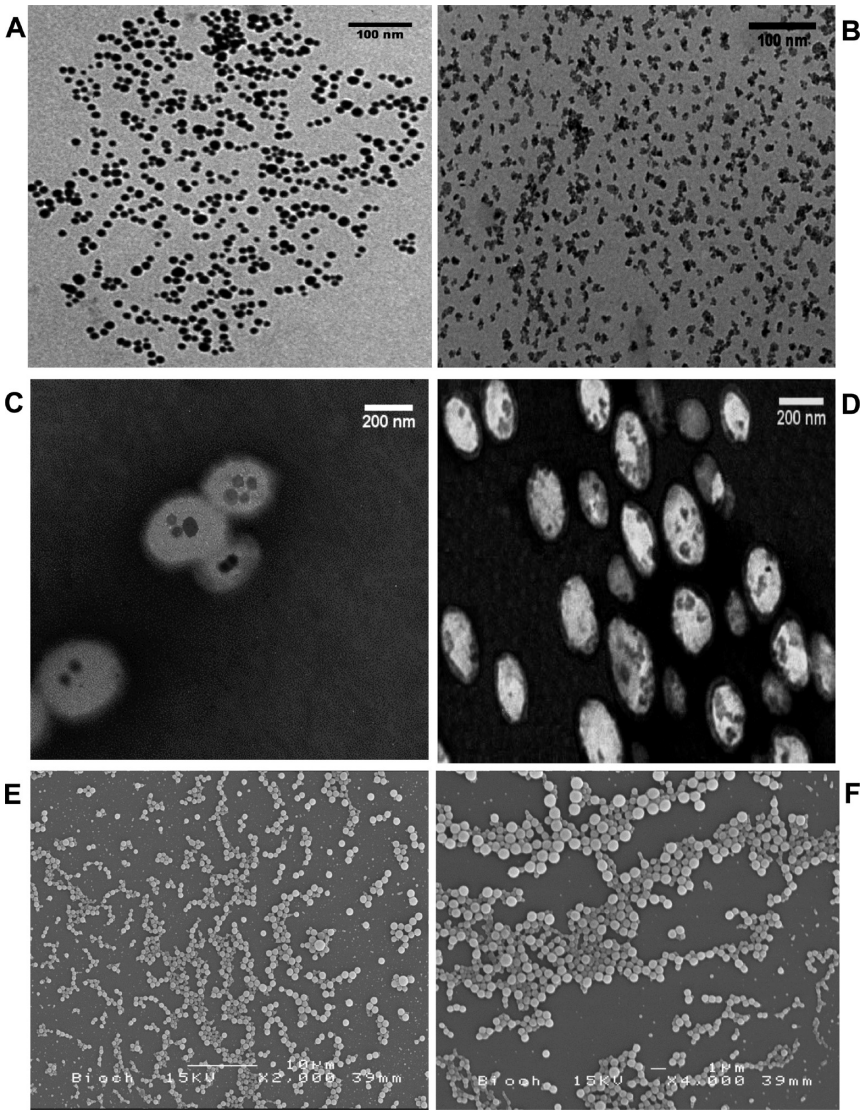

Figure 2. PLGA NP carriers contain SPIO and gold nanoparticles. (A) TEM image of representative gold nanospheres. Sodium citrate was used as the reducing agent. (B) TEM image of representative SPIO nanospheres. (C) TEM image of a representative PLGA harboring gold NPs. (D) TEM image of a representative PLGA harboring SPIO. Image analysis revealed the electron-dense gold and SPIO nanospheres within the PLGA matrix and the presence of the PEG-lipid layer surrounding the NPs. (Scale bar, 200 nm; magnification, 30000×.) (E, F) PLGA analysis by SEM revealed nanosized spherical particle morphology.

NP uptake by flow cytometry on a FacsCalibur (Becton Dickinson, USA). In other experiments, histological analyses of popliteal and lumbar lymph nodes section were performed on isolated lymph nodes by Prussian blue staining.

2.19. In Vivo Antigen Presentation Experiments. C57Bl/6J and OT-I mice (Charles River) were maintained under specific pathogen-free conditions at the Central Animal Laboratory (Nijmegen, The Netherlands). Drinking water and food were provided ad libitum. The experiments were performed according to animal care guidelines of the Nijmegen Animal Experiments Committee.

Targeted or nontargeted PLGA NPs were iv injected into tail veins of C57Bl/6J mice. Three days later (2−3) × 10^6 CFSE-labeled OVA-specific $CD8^+$ T cells derived from OT-1 mice were injected iv. At day 6, the mice were sacrificed and spleens were isolated. Single cell suspensions were made and analyzed by flow cytometry after staining with fluorophore-coupled Abs to CD4, CD8, and the OT-1 TCRVα2 (BD Pharmingen).

2.20. Statistics. Graph Pad Prism software version 5 was used for statistical analysis. Data were analyzed by one-way ANOVA followed by Newman−Keuls post test or a two-way ANOVA followed by Bonferroni post test.

3. RESULTS AND DISCUSSION

3.1. Design, Preparation, and Characterization of Nanoparticles. The tetanus toxoid (TT) 830−844 peptide was covalently linked to the fluorophore FITC (FITC-TT), by solid-phase synthesis.[22,23] This allows visualization of peptide conjugated to SPIO or gold, either free or incorporated into PLGA NPs, and visualizing human DCs associated with the peptide antigen. Two additional changes were made at both the *C*- and the *N*-terminus. Thus, a Cys residue was added at the *C*-terminus of certain TT peptides to allow grafting onto the gold surface of NPs by covalent bonding. *N*-Terminal modification was carried out with FITC to allow tracking by confocal microscopy and flow cytometry (Figure 1A).

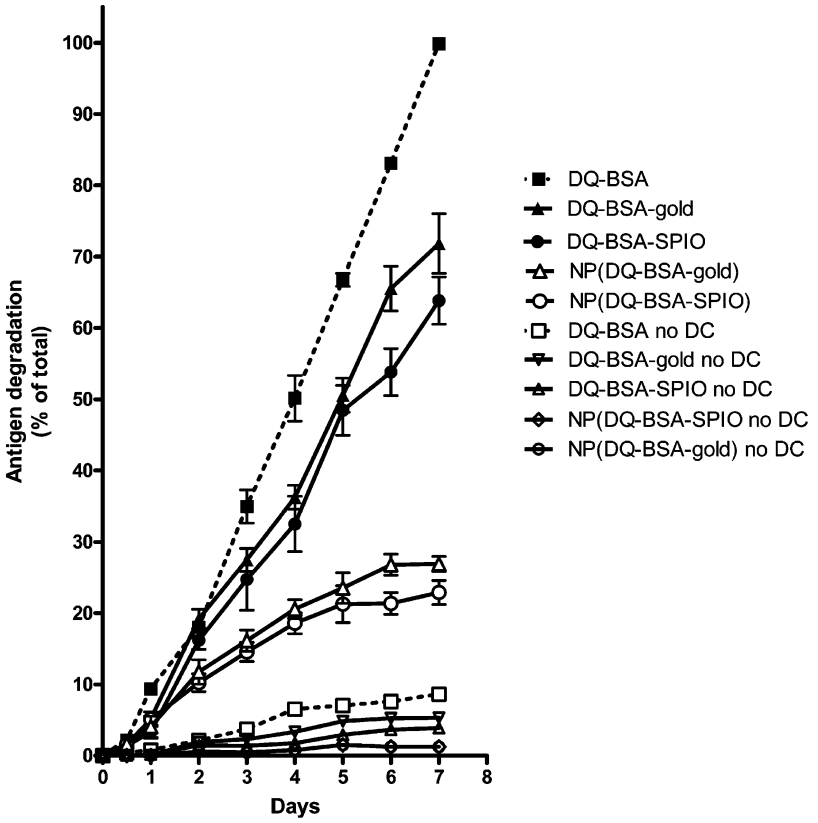

Figure 3. Antigen degradation kinetics of the distinct nanoparticles. Distinct combinations of antigen and PLGA NPs were tested. DQ-BSA was used as self-quenching protein. The release and degradation of protein antigen coupled to SPIO and gold nanoparticles, either free in solution or encapsulated within PLGA-NPs, was tracked for 7 days. Self-quenching model protein antigen DQ-BSA was incubated in culture medium in the presence or absence of human DCs as experimental control. Data represent the mean value ± SD from three independent experiments performed in quadruplicate.

Furthermore, we also exploited superparamagnetic NPs. Initially, SPIO NPs of 8.2 ± 1.5 nm in diameter were conjugated to the FITC-TT peptide (Figure 1A). The conjugation of FITC-TT peptide to SPIO was confirmed by measuring particle-associated fluorescence. A similar strategy was used for Atto-647-OVA and DQ-BSA. Thus, we also conjugated Atto-647-OVA and DQ-BSA protein to SPIO via amide bond as described above.[24] The physicochemical characteristics of fluorescently labeled antigen-SPIO or -gold NPs are shown in Table 1.

Next, the fluorescently labeled antigen-SPIO or -gold nanospheres were encapsulated within PLGA NPs using a single emulsion method. These PLGA NPs containing antigen together with contrast agents and fluorescent antigens were generated for optical imaging, MRI, and immunological studies on the cellular and organism level (Figure 1B).

The PLGA NP surface was coated with a polyethylene glycol (PEG)-lipid layer to allow the incorporation of a DC-specific Ab to effectively target human and mouse DCs (Figure 1C). The characteristics of targeted PLGA NPs containing fluorescent antigen-SPIO and gold NPs (size distribution, polydispersity index, zeta potential, fluorescent antigen entrapment efficiency, SPIO and gold contents, and amount of Abs conjugated to PLGA NP surface) are shown in Table 2. Exploiting dynamic light scattering we found that the size of PLGA NPs harboring SPIO and gold varied from 199.4 ± 6.8 nm and 219.0 ± 5.1 nm without Abs to 225.6 ± 12.6 nm and 251.6 ± 10.9 nm with Abs, respectively. The polydispersity index was below 0.200 in all NP preparations (Table 2). In addition, the zeta potential of Ab-coated PLGA NPs was considerably less negative than that of the PLGA NPs without Abs (Table 2). The zeta potential value of noncoated PLGA NP-PEG-COOH was in the range of −29.5 ± 1.8 mV to −36.1 ± 1.7 mV while the values of PLGA NP-αDC-SIGN and isotype abs were in the range from −11.3 ± 1.6 mV to −16.9 ± 1.6 mV. The amount of Abs present on the particle surface was in the range 24.2 ± 2.4 μg to 27.6 ± 2.1 μg per mg of PLGA, as determined by a Coomassie-based protein assay (see Table 2). In addition, FACS analysis revealed that at least 90% of the NPs carry Abs on their surface (Figure S1 in the Supporting Information).

The morphology of all NPs was determined by TEM. Figures 2A and 2B show that the gold NPs were uniform in size and showed spherical shape, in contrast to SPIO NPs that showed some aggregation due to their intrinsic magnetic properties. TEM analysis revealed that the SPIO and gold are present within PLGA NPs (Figure 2C,D). In addition, TEM imaging clearly shows the presence of the PEG-lipid layer on the PLGA NPs in both preparations. In addition, SEM confirmed that the PLGA NPs are uniform and spherical in shape. In general, the SEM images have lower resolution than TEM images (Figure 2E,F).

A combination of different techniques was exploited to demonstrate the bimodal imaging properties (fluorescence and magnetic resonance) of the PLGA NPs: Flow cytometry and confocal imaging clearly confirmed the encapsulation of FITC-TT peptide within PLGA-NPs (Figure S2A,B in the Supporting

dx.doi.org/10.1021/mp400717r | Mol. Pharmaceutics XXXX, XXX, XXX−XXX

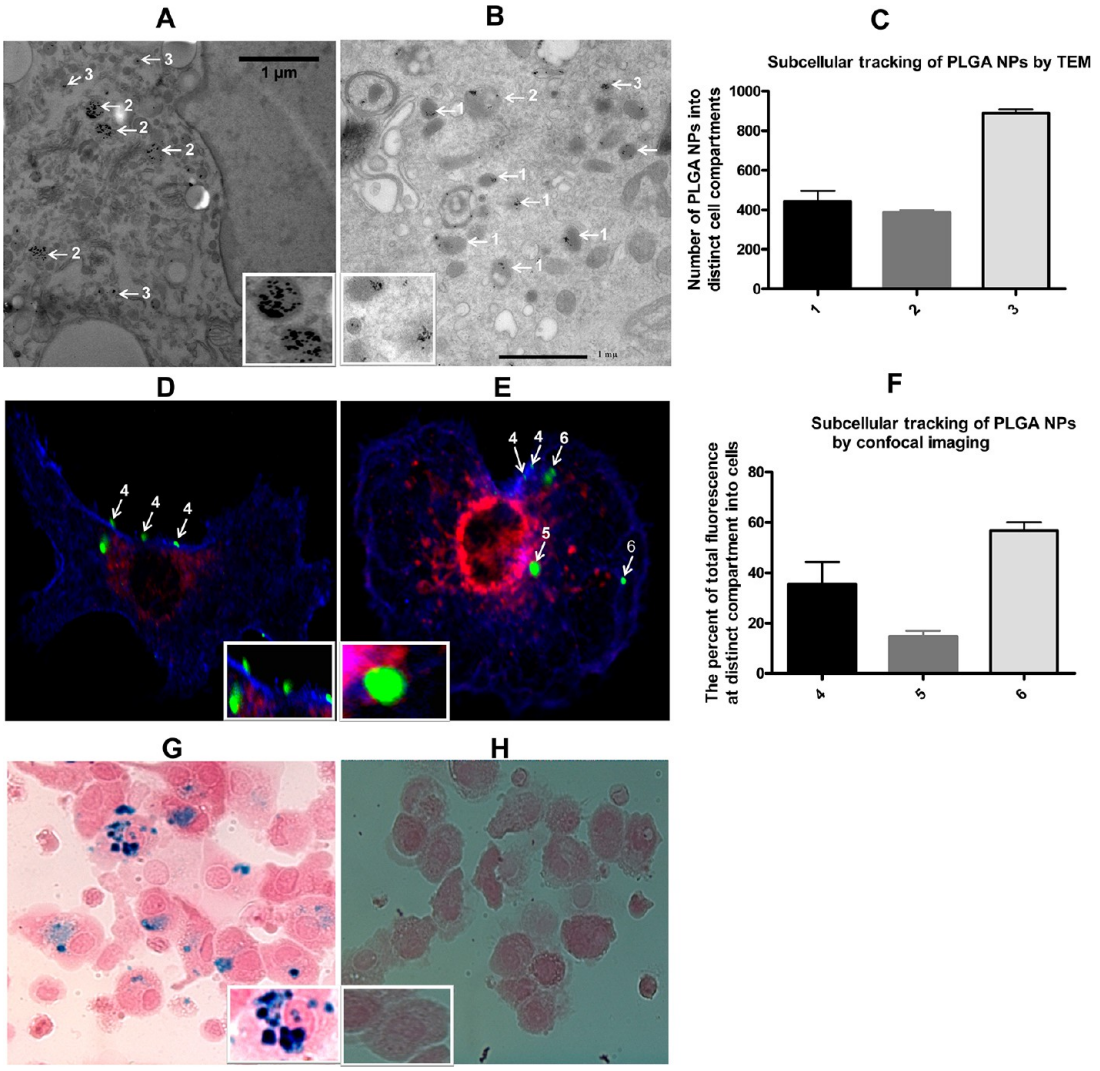

Figure 4. Subcellular tracking of PLGA NPs by TEM, confocal imaging, and Prussian blue staining. DCs were incubated with targeted PLGA NPs NP(FITC-TT-SPIO)-αDC-SIGN and NP(FITC-TT-gold)-αDC-SIGN for 1 h and chased for 24 h. Subsequently, cells were analyzed by intracellular TEM picture (A and B). For TEM studies DCs were embedded and analyzed. (A) The PLGA NPs harboring SPIO and (B) gold nanoparticles could be distinguished by their morphology from intracellular organelles. (1) Part of the PLGA NPs was found in the endocytic vesicles; (2) a proportion of the SPIO or gold was already released from NPs and associated with endosomal or lysosomal membranes; (3) other NPs were localized within the cytoplasm. (C) Quantification of PLGA NPs at distinct subcellular compartments in several cells. (D) Binding and (E) uptake for confocal laser scanning microscopy, DCs were stained for the lysosomal marker LAMP1 (red) and DC-SIGN (neck-specific αDC-SIGN Ab DCN46 (blue)) and isotype-specific, AlexaFluor-conjugated secondary Abs. PLGA NPs harboring FITC-TT peptide appear green. Subsequently, cells were analyzed using an Olympus FV1000 confocal laser scanning microscope. (4) Targeted PLGA NPs are binding to the DC-SIGN receptor; (5) targeted PLGA NPs were partially colocalized with LAMP1 positive compartments; (6) part of the PLGA NPs did not colocalize with LAMP1. (F) The percentage of total fluorescence at distinct subcellular compartments was measured by ImageJ. Histological analysis of DCs (G) incubated with NP(SPIO)-αDC-SIGN for 24 h at 37 °C or (H) untreated cells. Cells were stained with Prussian blue staining to detect SPIO (blue). Cell nuclei are stained red. Magnification, 60×.

Information) while encapsulated SPIO and gold could be traced by MRI (Figure S2C in the Supporting Information).

3.2. Intracellular DQ-BSA Ag Degradation Kinetics of the Various PLGA NPs in Living Cells. We previously devised an assay to follow release and subsequent degradation of an encapsulated model protein antigen, DQ-BSA, in living cells in vitro using fluorescence.[25] Here, we used this assay to examine protein antigen degradation, conjugated to SPIO and gold particles, free or encapsulated within PLGA NPs, following uptake by DCs (Figure 3). As expected, free soluble antigen was degraded faster than antigen conjugated to SPIO and gold particles. Encapsulation within PLGA NPs further reduced degradation of antigen conjugated to SPIO or gold particles, showing that both conjugation and encapsulation protects antigen from rapid degradation. Slow degradation is favorable for both antigen presentation and the ability to track carriers following uptake by DCs by MRI over a prolonged period of time.

3.3. Intracellular Localization Detected by Transmission Electron Microscopy, Confocal Imaging, and Prussian Blue Staining. To investigate if the PLGA NPs harboring SPIO and gold can be tracked at the subcellular level, these particles were incubated with DCs for 24 h. The intracellular fate of the PLGA NPs was accessed by electron microscopy, using the encapsulated SPIO and gold particles as contrast agents. Electron dense SPIO and gold structures could

dx.doi.org/10.1021/mp400717r | *Mol. Pharmaceutics* XXXX, XXX, XXX−XXX

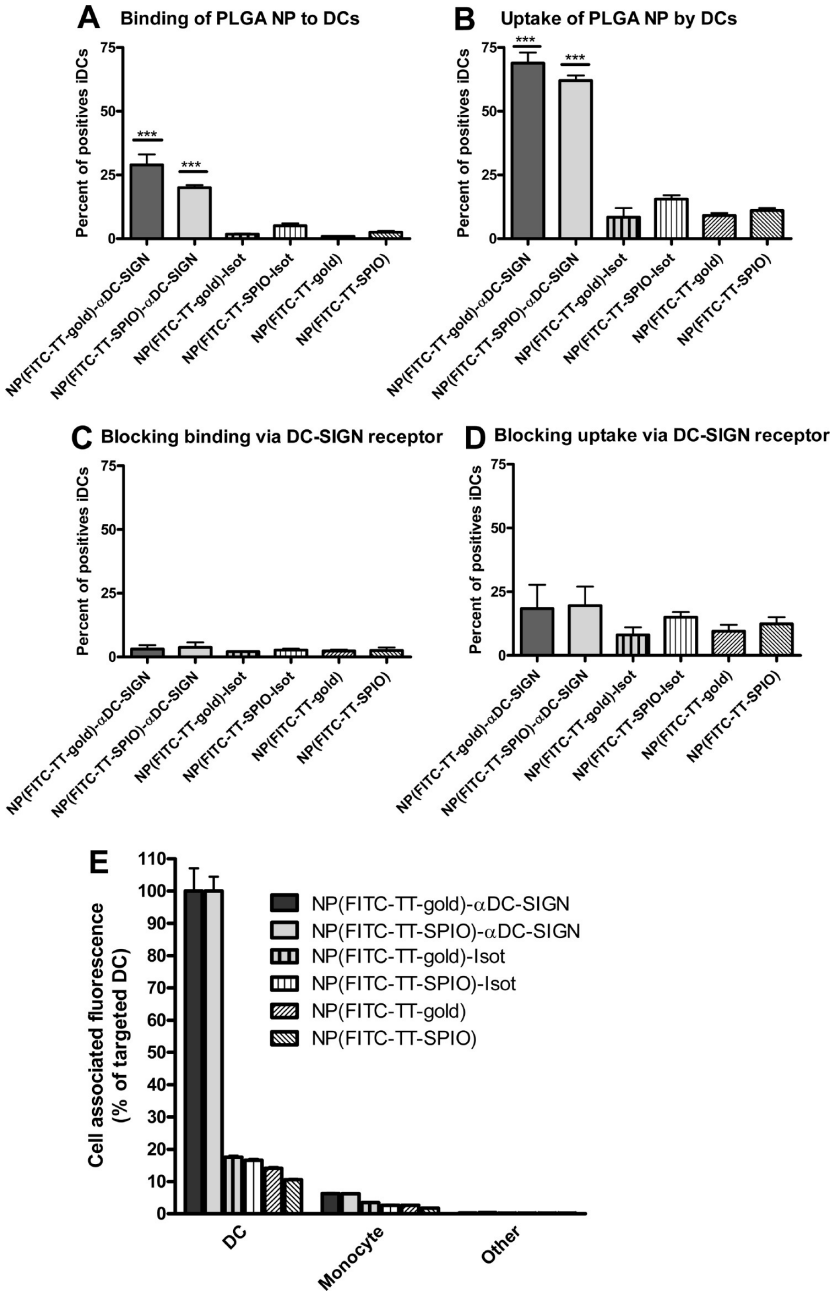

Figure 5. Analyzing PLGA NP carrier binding, uptake, and selective uptake in a mixture of cell types. Binding of various PLGA NP carriers was determined by (A) flow cytometry using NP(FITC-TT-SPIO)-αDC-SIGN, NP(FITC-TT-gold)-αDC-SIGN, NP(FITC-TT-SPIO)-isotype, NP(FITC-TT-gold)-isotype, and PLGA NPs without Abs incubated with DCs for 1 h at 4 °C. DCs cultured in medium without NPs were included as a negative control. (B) Subsequently, the experiments were repeated at 37 °C to study PLGA NP uptake by DCs for 1 h. Flow cytometry data represent the mean of experiments performed in triplicate ± SD. To determine the specificity of PLGA NP carrier binding and uptake, experiments were performed with preblocking of DC-SIGN receptor (C, D). Differences in binding and uptake were analyzed applying one-way ANOVA with Bonferroni post tests, ** = $p < 0.01$. (E) The selectivity of the uptake of each type of PLGA NPs by DCs was tested in a culture system comprising multiple cell subsets present in human blood. Distinct PLGA NPs were incubated with human leukocytes and DCs (ratio 20:1) and cultured for 2 h at 37 °C. Next, the mean cell fluorescence of the DCs, the monocytes, and the remaining leukocytes was determined by flow cytometry; the indicted values represent experiments performed in duplicate ± SD.

be seen by TEM in DCs exposed to targeted PLGA NPs NP(FITC-TT-SPIO)-αDC-SIGN and PLGA NP(FITC-TT-gold)-αDC-SIGN (Figures 4A and 4B). SPIO and gold appeared more electron dense than PLGA and could be detected within PLGA NP structures. Intact PLGA NPs containing SPIO and gold were detected in the cytosol of DCs, as characterized by the absence of an additional surrounding bilayer other than the one representing the PEG layer. Quantification of NPs at different subcellular compartments suggests that the majority of the PLGA NPs escaped from endosomal/lysosomal compartments to the cytosol (Figure 4C). Moreover, some PLGA NPs were found in endosomal structures. Surprisingly, to a small extent free SPIO and gold were found associated with endosomal membranes, suggesting that encapsulated SPIO and gold were released from

the NP carrier during the endocytosis process and associated with membrane structures.

Next, we exploited the bimodal properties of our NP(FITC-TT-SPIO)-αDC-SIGN to track and localize their routing inside DCs by confocal microscope. Adherent DCs were loaded with PLGA NPs for binding at 4 °C for 1 h and incubated for another 1 h at 37 °C for uptake. Subsequently, DCs were stained with the neck-specific αDC-SIGN Ab DCN46 for the membrane receptor and the late endosomal/lysosomal marker LAMP1, to visualize the binding via DC-SIGN receptor and the lysosomal compartment (Figure 4D,E). PLGA NP-derived fluorescence did colocalize with DC-SIGN receptor, showing that targeted PLGA NPs bound the target receptor (Figure 4D). Within 1 h the PLGA NPs were internalized into the DCs and some were partially colocalized with LAMP1 positive compartments. However, part of the fluorescence did not colocalize with LAMP1 compartments (Figure 4E). Indeed, the percentage of the total fluorescence indicates that a high number of particles escaped from the lysosomal pathway (Figure 4F), in line with our TEM analysis (Figure 4C). It was previously suggested by us and others that PLGA NPs are able to cross the endosomal membrane and deliver encapsulated antigen into the cytoplasm.[26,27,18]

Moreover, we assessed whether the presence of SPIO containing PLGA NPs could be detected within DCs by histological analysis using Prussian blue staining to detect the iron. The DCs were loaded with targeted and untargeted PLGA and incubated during 24 h. Prussian blue staining confirmed that PLGA NPs containing iron oxide nanoparticles were internalized by DCs (Figures 4G and 4H as control).[28]

Together, these experiments confirmed the flow cytometry data on NP binding and uptake. Similarly, the intracellular uptake of PLGA NPs was confirmed by TEM, confocal imaging, and Prussian blue staining. TEM showed the presence of PLGA NP harboring SPIO and gold NPs inside of DCs after internalization. In line with TEM analysis, confocal imaging clearly showed the presence of FITC-TT peptide within PLGA NPs (Figure 4D,E), while the SPIO was detectable intracellular by Prussian blue staining (Figure 4G,H). Uptake of PLGA NPs containing SPIO was confirmed by Prussian blue staining. Taken together, by using confocal imaging and TEM, it was possible to demonstrate that targeted PLGA NPs harboring SPIO-FITC and gold-FITC labeled NPs are internalized within DCs. Whereas confocal analysis was useful to identify the nature of the lysosomal compartments containing the fluorescent PLGA NPs, TEM also suggested that part of the NPs had escaped into the cytosol and revealed intracellular release of part of the gold and SPIO from the PLGA matrix within 24 h. This confirms that PLGA is slowly degraded within DCs.[29]

3.4. Specific Binding and Uptake of the PLGA NPs by DC. PLGA NPs containing SPIO and gold coated with anti-DC-SIGN Ab bound to DCs, while PLGA NPs with isotype control or no Abs hardly associated with DCs (Figure 5A). These data showed that targeted PLGA NPs mainly bind DCs via DC-SIGN and not through nonspecific interactions resulting from the surface charge or via nonspecific Fc receptor binding. This result is in line with the confocal picture shown in Figure 4C, where we demonstrated the binding PLGA NP via DC-SIGN receptor.

Furthermore, the capacity of the DC-targeted PLGA NPs to deliver their contents inside the cell was investigated. After 1 h at 37 °C, the uptake of NP(FITC-TT-gold)-αDC-SIGN (62%) and NP(FITC-TT-SPIO)-αDC-SIGN (60%) was higher than that of the corresponding NP-isotype control Ab (10% and 15%, respectively) or no Ab (11%) according to FACS analysis (Figure 5B). We also demonstrated that the PLGA NP uptake can be monitored by MRI (see Figure S3 in the Supporting Information). Furthermore, our result is in line with the confocal image in Figure 4E, where we demonstrated the uptake PLGA NP via DC-SIGN receptor. Binding and uptake of PLGA NP vaccines harboring specific DC-SIGN Abs was inhibited by preblocking the DC-SIGN domain with Abs. As expected, blocking DC-SIGN domain hardly affected binding and uptake of PLGA NPs (Figure 5C and D).

To investigate how efficiently and specifically the PLGA NP carriers target to DCs in the presence of other cell types (such as present in the bloodstream), we determined the binding and uptake of our PLGA NP carrier within a mixed blood cell population. Monocyte-derived DCs were mixed with freshly isolated leukocytes from blood of healthy human donors at a ratio of 1:20. PLGA NPs targeted to DCs via DC-SIGN were internalized more efficiently than untargeted controls NPs (Figure 5E). These results demonstrate that, despite low levels of unspecific uptake of PLGA NPs by DCs, targeting of DC-specific receptors by Abs on the particle surface strongly stimulate specific binding and uptake.

3.5. Targeted PLGA NP Harboring Fluorophore-Antigen Conjugated to SPIO or Gold Is Processed Efficiently by DCs and Presented to T Cells. Antigen presentation studies were performed to determine whether the bimodal imaging strategy was compatible with antigen presentation. DCs from donors that respond to TT-antigen were exposed to targeted and untargeted PLGA NPs and incubated with autologous T cells. Despite the facts that FITC-TT was conjugated to SPIO or gold particles and that FITC was linked to the peptide antigen, DCs presented the encapsulated antigen to T cells, resulting in T cell proliferation (Figure 6A,B). Particles coated with αDC-SIGN induced T cell proliferation in a dose dependent fashion, whereas the isotype control coated PLGA NPs did not induce T cell proliferation at the tested concentrations. These results are in agreement with our previous data, showing enhanced presentation of non-conjugated antigen targeted to DC-SIGN.[17]

3.6. Tracking of DC Migration Loading with Labeled Bimodal PLGA NPs. To explore the DC migration capacity after loading with bimodal NPs, we evaluated the migration of human DCs preloaded with NP(FITC-TT-SPIO)-αDC-SIGN or NP(FITC-TT-gold)-αDC-SIGN. Collagen scaffolds were used to mimic human tissue. The experimental setup is schematically plotted in Figure 7A. An empty basal collagen layer is positioned at the bottom. A scaffold gel layer with DCs is placed on top of the collagen layer. The potential migration region was positioned on top of the DC layer, consisting of a collagen layer containing a chemokine gradient. This setup should induce DC migration in the direction of the chemokine gradient. Immediately after the whole sample was set, cell migration was tracked by optical microscopy and video camera. Figures 7B and 7C show no significant differences in migration dynamics of NP(FITC-TT-gold)-αDC-SIGN and NP(FITC-TT-SPIO)-αDC-SIGN labeled compared to unlabeled control cells. However, the mobility of DCs loaded with NP(FITC-TT-SPIO)-αDC-SIGN was reduced compared with NP(FITC-TT-gold)-αDC-SIGN loaded DCs in all three replicate experiments.

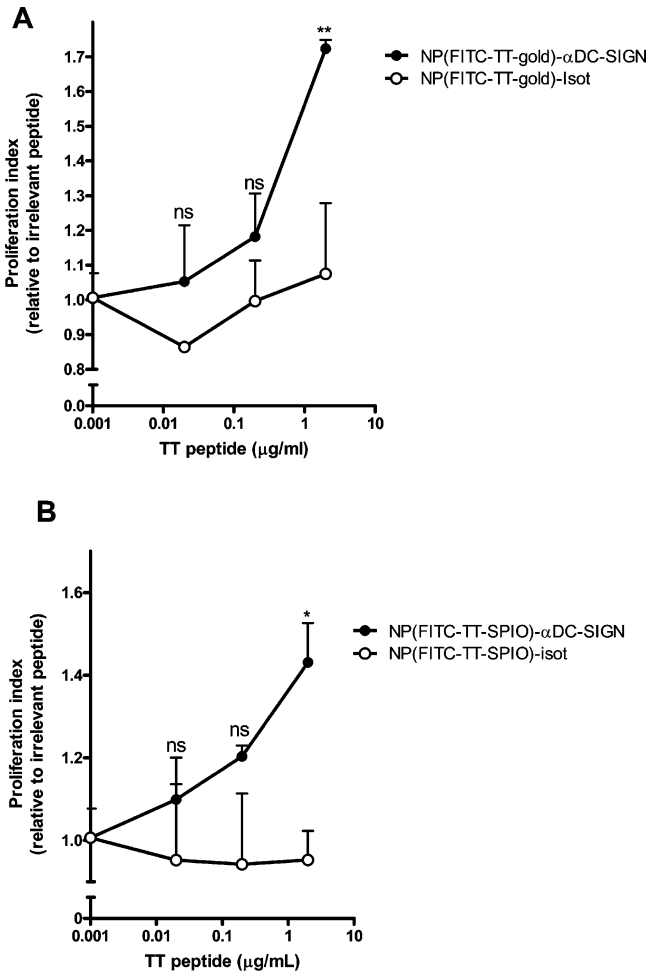

Figure 6. Specific targeting of PLGA NPs to human DCs enhances antigen presentation. Presentation of TT peptide was studied by culturing mature DCs for 2 days in medium with or without addition of various concentrations of (A) NP(FITC-TT-gold)-αDC-SIGN (closed circles) or NP(FITC-TT-gold)-isotype (open circles) and (B) NP(FITC-TT-SPIO)-αDC-SIGN (closed circles) or NP(FITC-TT-SPIO)-isotype (open circles). Subsequently, autologous TT-responsive PBLs were added. After 4 days, cellular responses were assessed in a proliferation assay. Data are mean proliferation indices ± SD relative to medium control for three experiments. Differences in T cell proliferation was analyzed applying two way ANOVA with Bonferroni post tests, * = $p < 0.05$ and ** = $p < 0.01$.

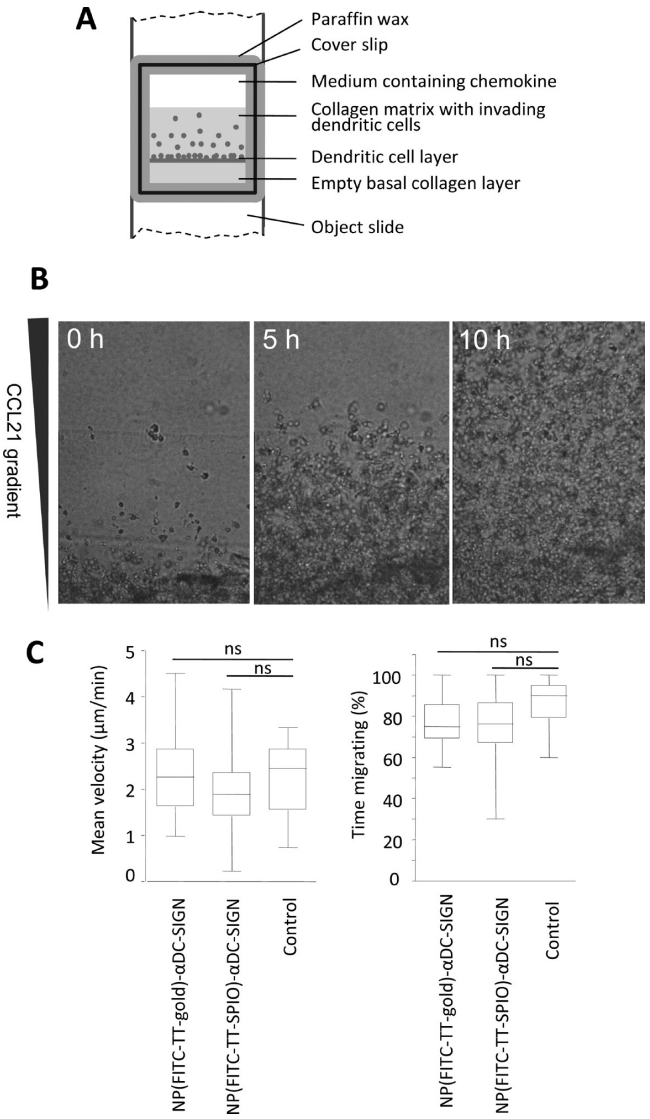

Figure 7. Loading of DC with bimodal PLGA NPs does not affect migration rates in 3D collagen matrices. (A) Migration chamber setup. Chambers were positioned upright and overlaid with CCL21 to apply a chemokine gradient inducing cell migration. (B) Migration of mature DC into the cell-free zone monitored by bright-field time-lapse microscopy. Images of consecutive time points show the upward migration toward the CCL21 gradient. (C) Migration activity assessed by cell tracking. Average velocity and percentage of time the cells were actively migrating were quantified from populations of 60 cells (two independent pooled experiments). Statistical analysis was performed using the two-tailed Student's *t* test for three independent experiments.

Two conclusions can be drawn from this experiment. First, ex vivo cultured human DCs were efficiently labeled with our targeted bimodal PLGA NPs and allowed tracking of cell migration. Second, the bimodal PLGA NPs did not abolish DC migration toward chemokines, which is important for DC migration toward the lymph nodes where they present antigen to T cells and induce immune responses. This is in contrast to other studies which have shown that SPIO (without PLGA) does affect cell migration capacity.[30]

3.7. Targeting of PLGA NP to Mouse DCs Enhances T Cell Proliferation and IFN-γ Production in Vitro. To investigate the influence of targeting our bimodal particles to mouse DCs using an Ab, we performed an antigen presentation assay in vitro. Since in mice DC-SIGN is not expressed in the cross-presenting CD8+ DC subset and its expression in monocyte-derived DCs is mostly located intracellular,[31] it is not an ideal target in the murine setting. Therefore, we chose to target DEC-205 as a DC-specific receptor in mice. We also replaced the FITC label on the antigen by Atto-647 to reduce nonspecific background signals during in vivo imaging. Bone marrow-derived dendritic cells (BMDCs) were incubated with bimodal particles that contained Atto-647-labeled ovalbumin (OVA) as the antigen, which was conjugated to SPIO. PLGA NPs bound specifically to the DEC-205 receptor on BMDCs (see Figure S4 in the Supporting Information). BMDCs were used on day 9 or day 16, and their purity was determined by staining with CD11c and Gr1; 80% of the cells were CD11c positive, and only 5% were Gr1 positive (data not shown). Next, BMDCs treated with targeted and nontargeted PLGA NPs were cocultured with either OT-1 or OT-2 T cells, which

dx.doi.org/10.1021/mp400717r | *Mol. Pharmaceutics* XXXX, XXX, XXX–XXX

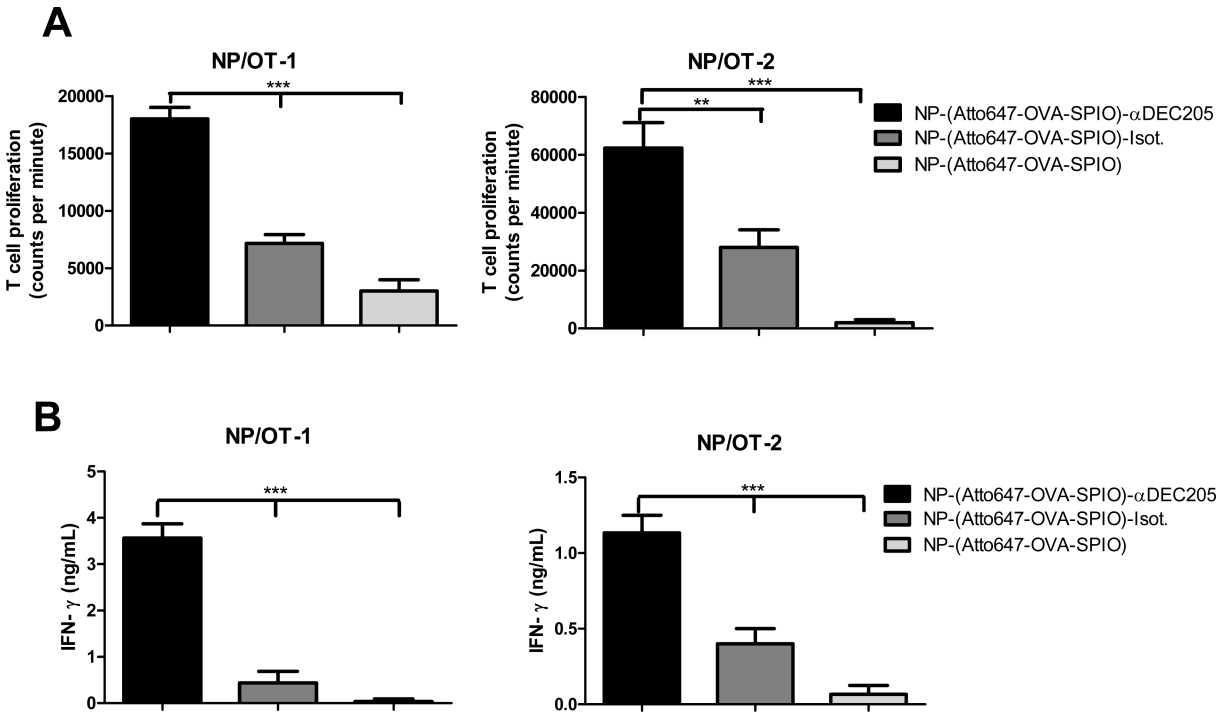

Figure 8. Targeted PLGA NPs enhance T cell proliferation and IFN-γ production. BMDCs were incubated with targeted and nontargeted PLGA NPs at 4 °C for 1 h; T cells were added and incubated with the BMDCs for 3 days. T cell proliferation was measured by the amount of incorporated tritium thymidine, and IFN-γ was used as a measure for T cell activation. (A) T cell proliferation of OT-1 and OT-2 cells and (B) IFN-γ production of OT-1 and OT-2 cells. As a negative control DCs in medium without addition of antigen were used. Data shown are means of 3 samples ± SD. Differences in OT-1 and OT-2 cell proliferation and IFN-γ production were analyzed applying two way ANOVA with Bonferroni post tests, ** = $p < 0.01$ and *** = $p < 0.001$.

express T cell receptors recognizing OVA in the context of MHC class I and MHC class II, respectively. After 3 days of incubation, T cell proliferation was measured by tritium thymidine incorporation. T cell activation was determined by measuring IFN-γ production by ELISA. We clearly observed that specific targeting of the bimodal PLGA NPs enhanced T cell proliferation and IFN-γ production in both OT-1 and OT-2 cells (Figure 8A,B). This indicates that specific binding to DEC-205 enhances BMDC loading with antigen resulting in improved antigen presentation to T cells. Also these results demonstrate that targeting is effective both in human and in mouse models. These results are in line with our previous work.[32]

3.8. Targeting Bimodal PLGA NPs to DCs Has Limited Effect on Tissue Biodistribution, but Enhances DC Loading and Subsequent T Cell Activation. After our observations in vitro that targeting of bimodal PLGA NP increases T cell proliferation and activation, we wanted to investigate the in vivo situation. Therefore, we performed an in vivo OT-1 cell proliferation assay following immunization of mice with targeted and nontargeted OVA-containing PLGA NPs. Figure 9A shows that, consistent with the in vitro situation, bimodal PLGA NPs targeted to the DC-specific receptor DEC-205 enhanced T cell proliferation compared to uncoated and isotype Ab-coated PLGA NPs.

In vivo and ex vivo analyses were performed to determine whether targeting enhanced T cell proliferation by affecting biodistribution and/or nanovaccine uptake by DCs. Therefore, the popliteal and lumbar lymph nodes were isolated 24 h after injection and single cell suspensions were prepared. DCs were stained and analyzed by flow cytometry to quantify antigen uptake by measuring Atto-647 OVA fluorescence. Figures 9B and 9C show that DCs had internalized significantly more nanovaccine PLGA NPs when they carried DC-specific antibodies. However, no obvious differences in tissue biodistribution of targeted, nontargeted, or isotype control coated PLGA NPs were observed after 24 h (Figure 9D). This suggests that, despite the fact that high numbers of NPs drain freely throughout the body and are available for uptake, nanovaccines are more efficiently scavenged by DCs when carrying receptor-specific Abs.

3.9. Visualization of Bimodal PLGA NPs in Vivo by MRI and Optical Imaging. After having imaged targeted and nontargeted nanovaccines at the level of cells and tissues, we tracked bimodal PLGA NPs at the organism level by visualizing them using MRI and optical imaging simultaneously. We performed footpad injections with either PLGA NPs harboring Atto-647-OVA-SPIO coated with αDEC205 or isotype Abs on the NP surface and followed their distribution for up to during 24 h. Figure 10A shows the kinetic trajectory of PLGA NPs by MRI indicating the presence of particles in the lymph node just 2 h after footpad injection. In addition, the fluorescent signal was detected in the popliteal and lumbar lymph node 3 h after injection using the FluorVivo (Figure 10B). The results suggest that these 200 nm sized nanovaccines drained freely through the lymphatic system and accumulated within the nodes. This was confirmed by histological analysis of lymph nodes using Prussian blue staining to stain for SPIO, which confirmed the presence of numerous NPs within the lymph node interstitium, irrespective of the fact whether they were targeted or not (Figure 10C,D).

dx.doi.org/10.1021/mp400717r | Mol. Pharmaceutics XXXX, XXX, XXX–XXX

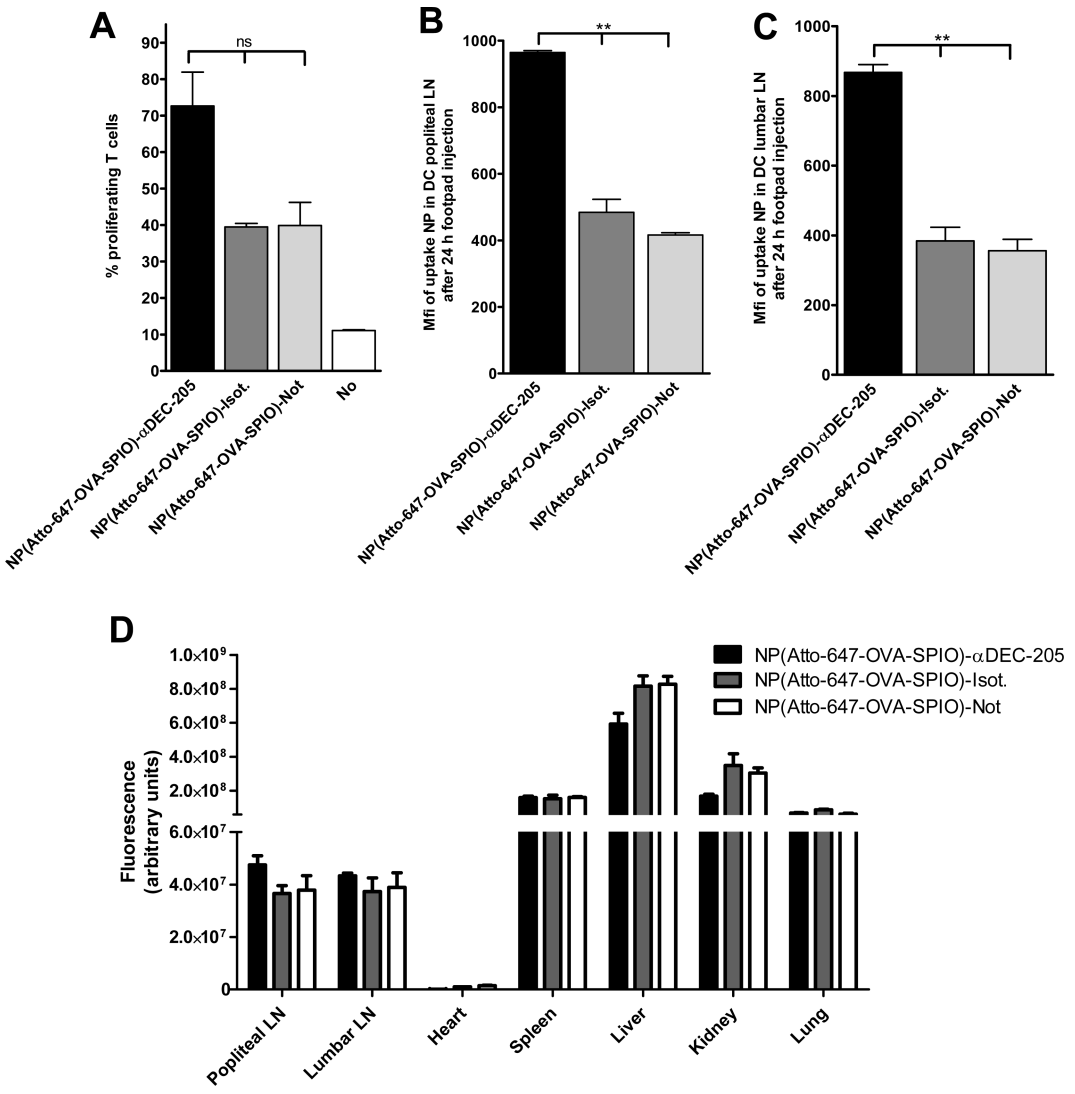

Figure 9. Targeting NPs to DCs enhances T cell proliferation and specific uptake in vivo, but hardly affects tissue distribution. Mice were vaccinated iv with 3 μg of OVA antigen encapsulated in PLGA NPs coated with αDEC205-specific Ab (DEC205) or isotype control Ab (isotype) or without Ab coating (uncoated). Control mice were injected with PBS without NPs (No). To determine CD8+ T cell proliferation, CFSE-labeled OVA-specific OT-1 CD8+ T cells were injected and 3 days later lymph nodes were harvested. OT-1 T cell proliferation was assessed by FACS analysis. Histograms show proliferation as measured by CFSE dye dilution in OT-I T cells. (A) Data represent means ± SEM of three independent experiments with two mice per group. Bimodal PLGA NPs harboring Atto-647-OVA-SPIO and coated with specific αDEC-205 or isotype Ab were injected iv in the mice. NPs contained 10 μg of Atto-647-OVA. Mice were sacrificed 24 h postinjection, and the popliteal and lumbar lymph nodes were harvested. Lymph node single cell suspensions were stained with labeled antibodies to distinguish the different immune cell populations positive for Atto-647 by flow cytometry. (B, C) The quantification of PLGA NP uptake per cell was based on mean fluorescent intensity (mfi) of DCs. The values were determined for each group depicted as mean ± SEM. Data were analyzed by one-way ANOVA with Bonferroni post tests, ** = $p < 0.01$. D) Mice were sacrificed 24 h postinjection, and fluorescence of all main organs was measured by FluorVivo. Tissue biodistribution profile of targeted and nontargeted bimodal PLGA NPs harboring Atto-647-OVA was determined. (D) Relative fluorescent values were determined for each group depicted as mean ± SEM.

4. CONCLUSIONS

We compared NPs consisting of a biocompatible polymer containing SPIO or gold covalently attached to fluorescently labeled antigen as a bimodal imaging contrast agent. We demonstrated that SPIO and gold were successfully encapsulated within our targeted PLGA NPs. Coating PLGA NPs with DC-specific DC-SIGN Abs significantly increased SPIO and gold uptake as compared to nontargeted controls in vitro. Moreover, Prussian blue staining and confocal microscopy provide additional information on cellular and subcellular localization of the PLGA NPs. We also show that loading the DCs with bimodal particles does not abolish cell migration in 3D scaffolds. Moreover, the presence of imaging agents did not hamper processing of encapsulated antigen and presentation to T cells. The results showed that PLGA NPs reach the popliteal lymph node within 2 h after injection, regardless of whether they were targeted or nontargeted. This suggests that the majority of NPs drained freely through the lymphatic conduits and did not depend on uptake by local, tissue-resident DCs and subsequent cellular migration to the lymph node. On tissue level, no differences were observed in routing between targeted and nontargeted PLGA NPs, and there was no clear evidence of enhanced retention of targeted NPs within lymph nodes. This seemed in contrast to the enhanced T cell responses induced by

dx.doi.org/10.1021/mp400717r | Mol. Pharmaceutics XXXX, XXX, XXX–XXX

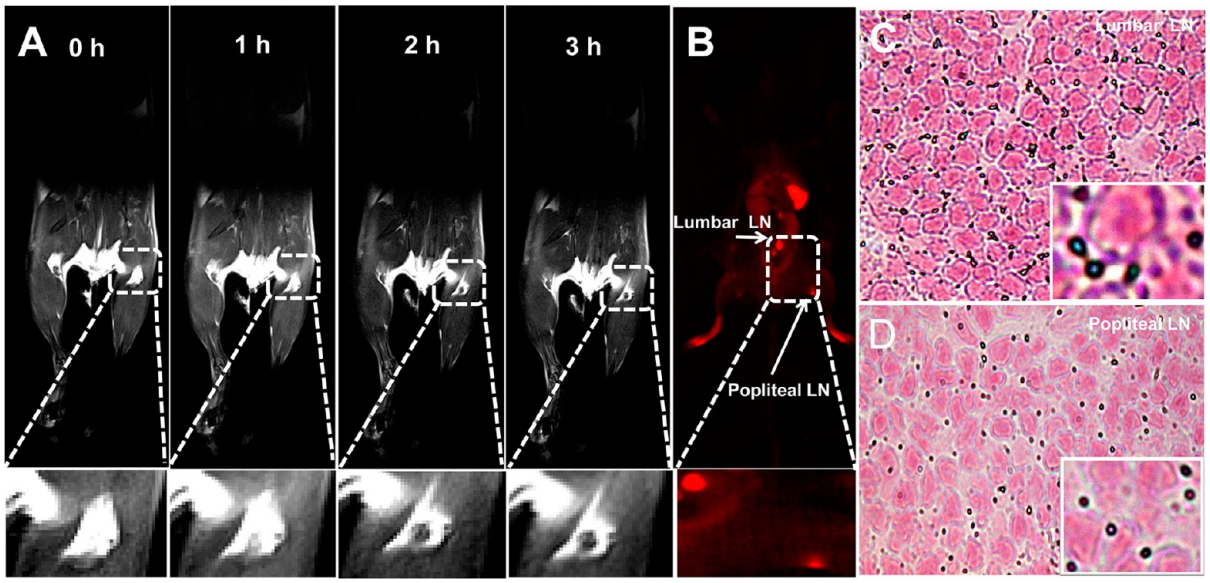

Figure 10. Tracking bimodal PLGA NPs in vivo by MRI and optical imaging. Bimodal PLGA NPs harboring Atto-647-OVA-SPIO and coated with αDEC-205 or isotype control Ab were injected in the mouse footpad. Injected PLGA NPs contained 10 μg of Atto-647-OVA. The PLGA NPs were monitored at various time points (1, 2, and 3 h) by MRI (A). FluorVivo analysis was performed 4 h postinjection (B). The inset represents a schematic overview of the used particles. Histological and Prussian blue staining of the different lymph nodes were performed (C, D). Panels display sections stained with Prussian blue revealing PLGA NPs containing SPIO.

targeted NPs and to the fact that analysis of lymph node cells ex vivo revealed that DCs take up more NPs carrying DC-specific antibodies. Histological analysis showed that large numbers of targeted and nontargeted PLGA NPs were located inside the lymph node area. Together, these data suggest that, upon injection, the majority of PLGA NPs pass through lymph nodes without being taken up by DCs. The presence of a DC receptor-specific antibody facilitates recognition of the PLGA NPs by DCs and enhances uptake and subsequent immunological responses. Targeted PLGA NPs represent a valuable tool to study diverse cellular processes at the subcellular, cellular, and organism levels, such as receptor biology, antigen processing, and presentation, as well as biodistribution of targeted vaccines and DC migration in vivo.

■ ASSOCIATED CONTENT

Supporting Information

Figures S1 (quantification of antibody on the PLGA-NP by flow cytometry), S2 PLGA NP contains bimodal imaging properties), S3 (uptake of PLGA NP by DCs measured by MRI), and S4 (binding of PLGA NP to BMDCs). This material is available free of charge via the Internet at http://pubs.acs.org.

■ AUTHOR INFORMATION

Corresponding Authors

*(L.J.C.) Experimental Molecular Imaging, Department of Radiology, Bldg. 1, C5-60, Leiden University Medical Center, Albinusdreef 2 2333 ZA Leiden, The Netherlands. Tel: +31 71 5263025. E-mail: l.j.cruz_ricondo@lumc.nl.

*(C.G.F.) Department of Tumor Immunology, Nijmegen Centre for Molecular Life Sciences, Radboud University Nijmegen Medical Centre, Postbox 9101, 6500 HB Nijmegen, The Netherlands. Fax: +31-24-3540339. Tel: +31-24-3617600. E-mail: c.figdor@ncmls.ru.nl.

Notes

The authors declare no competing financial interest.

■ ACKNOWLEDGMENTS

The authors wish to thank the technicians of the RIMLS Tumor Immunology Department Clinical DC group for assistance. This work is supported by a Marie Curie Research Training Network EU grant, Immunonamap (MRTN-CT-2006-035946), European Research Council (ERC) Grant ERC02010-AdG-269019-PATHFINDER and ERC-2104-StG-336454-CoNQUeST, the Netherlands Organization for Scientific Research (NWO) VENI 700.10.409 and a Spinoza award, and the Netherlands Institute of Regenerative Medicine (NRIM) FES0908, and the EU FP7 program ENCITE (HEALTH-F5-2008-201842).

■ ABBREVIATIONS USED

Abs, antibodies; DC, dendritic cell; DIEA, *N*,*N*-diisopropylethylamine; DIPCDI, *N*,*N*′-diisopropylcarbodiimide; DLS, dynamic light scattering; DCM, dichloromethane; DMF, *N*,*N*-dimethylformamide; EDAC, *N*-(3-(dimethylamino)propyl)-*N*-ethylcarbodiimide hydrochloride; FDA, food and drug administration; HOBt, 1-hydroxybenzotriazole; HPLC, high performance liquid chromatography; MRI, magnetic resonance imaging; MALDI-TOF, matrix-assisted laser desorption ionization with time-of-flight analysis; NP, nanoparticle; NHS, *N*-hydroxisuccinimide; PBL, peripheral blood lymphocyte; PBMC, peripheral blood mononuclear cell; PEG, polyethylene glycol; PLGA, poly(D, L-lactide-*co*-glycolide); PVA, poly(vinyl alcohol); RP, reverse phase; SEM, scanning electron microscopy; SPIO, superparamagnetic iron oxide particles; TEM, transmission electron microscopy; TFA, trifluoroacetic acid; TT, tetanus toxoid

■ REFERENCES

(1) Lesterhuis, W. J.; Aarntzen, E. H.; De Vries, I. J.; Schuurhuis, D. H.; Figdor, C. G.; Adema, G. J.; Punt, C. J. Dendritic cell vaccines in melanoma: from promise to proof? *Crit. Rev. Oncol. Hematol.* **2008**, *66* (2), 118–34.

(2) Schreibelt, G.; Klinkenberg, L. J.; Cruz, L. J.; Tacken, P. J.; Tel, J.; Kreutz, M.; Adema, G. J.; Brown, G. D.; Figdor, C. G.; de Vries, I. J. The C-type lectin receptor CLEC9A mediates antigen uptake and (cross-)presentation by human blood BDCA3+ myeloid dendritic cells. *Blood* **2012**, *119* (10), 2284−92.
(3) Kreutz, M.; Tacken, P. J.; Figdor, C. G. Targeting dendritic cells—why bother? *Blood* **2013**, *121* (15), 2836−44.
(4) Guo, R.; Li, R.; Li, X.; Zhang, L.; Jiang, X.; Liu, B. Dual-functional alginic acid hybrid nanospheres for cell imaging and drug delivery. *Small* **2009**, *5* (6), 709−17.
(5) Beaune, G.; Dubertret, B.; Clement, O.; Vayssettes, C.; Cabuil, V.; Menager, C. Giant vesicles containing magnetic nanoparticles and quantum dots: feasibility and tracking by fiber confocal fluorescence microscopy. *Angew. Chem., Int. Ed.* **2007**, *46* (28), 5421−4.
(6) McCarthy, J. R.; Jaffer, F. A.; Weissleder, R. A macrophage-targeted theranostic nanoparticle for biomedical applications. *Small* **2006**, *2* (8−9), 983−7.
(7) Mulder, W. J.; Griffioen, A. W.; Strijkers, G. J.; Cormode, D. P.; Nicolay, K.; Fayad, Z. A. Magnetic and fluorescent nanoparticles for multimodality imaging. *Nanomedicine (London)* **2007**, *2* (3), 307−24.
(8) Uzgiris, E. E.; Sood, A.; Bove, K.; Grimmond, B.; Lee, D.; Lomnes, S. A multimodal contrast agent for preoperative MR Imaging and intraoperative tumor margin delineation. *Technol. Cancer Res. Treat.* **2006**, *5* (4), 301−9.
(9) Veiseh, O.; Sun, C.; Gunn, J.; Kohler, N.; Gabikian, P.; Lee, D.; Bhattarai, N.; Ellenbogen, R.; Sze, R.; Hallahan, A.; Olson, J.; Zhang, M. Optical and MRI multifunctional nanoprobe for targeting gliomas. *Nano Lett.* **2005**, *5* (6), 1003−8.
(10) Quaranta, V.; Walker, L. E.; Pellegrino, M. A.; Ferrone, S. Purification of immunologically functional subsets of human Ia-like antigens on a monoclonal antibody (Q5/13) immunoadsorbent. *J. Immunol.* **1980**, *125* (4), 1421−5.
(11) Tacken, P. J.; de Vries, I. J.; Gijzen, K.; Joosten, B.; Wu, D.; Rother, R. P.; Faas, S. J.; Punt, C. J.; Torensma, R.; Adema, G. J.; Figdor, C. G. Effective induction of naive and recall T-cell responses by targeting antigen to human dendritic cells via a humanized anti-DC-SIGN antibody. *Blood* **2005**, *106* (4), 1278−85.
(12) Thomas, T. C.; Rollins, S. A.; Rother, R. P.; Giannoni, M. A.; Hartman, S. L.; Elliott, E. A.; Nye, S. H.; Matis, L. A.; Squinto, S. P.; Evans, M. J. Inhibition of complement activity by humanized anti-C5 antibody and single-chain Fv. *Mol. Immunol.* **1996**, *33* (17−18), 1389−401.
(13) Houghten, R. A.; Bray, M. K.; Degraw, S. T.; Kirby, C. J. Simplified procedure for carrying out simultaneous multiple hydrogen fluoride cleavages of protected peptide resins. *Int. J. Pept. Protein Res.* **1986**, *27* (6), 673−8.
(14) Kumar, C. S.; Leuschner, C.; Doomes, E. E.; Henry, L.; Juban, M.; Hormes, J. Efficacy of lytic peptide-bound magnetite nanoparticles in destroying breast cancer cells. *J. Nanosci. Nanotechnol.* **2004**, *4* (3), 245−9.
(15) Bradford, M. M. A rapid and sensitive method for the quantitation of microgram quantities of protein utilizing the principle of protein-dye binding. *Anal. Biochem.* **1976**, *72*, 248−54.
(16) Cruz, L. J.; Rueda, F.; Cordobilla, B.; Simon, L.; Hosta, L.; Albericio, F.; Domingo, J. C. Targeting nanosystems to human DCs via Fc receptor as an effective strategy to deliver antigen for immunotherapy. *Mol. Pharmaceutics* **2011**, *8* (1), 104−16.
(17) Cruz, L. J.; Tacken, P. J.; Fokkink, R.; Joosten, B.; Stuart, M. C.; Albericio, F.; Torensma, R.; Figdor, C. G. Targeted PLGA nano- but not microparticles specifically deliver antigen to human dendritic cells via DC-SIGN in vitro. *J. Controlled Release* **2010**, *144* (2), 118−26.
(18) Cruz, L. J.; Tacken, P. J.; Bonetto, F.; Buschow, S. I.; Croes, H. J.; Wijers, M.; de Vries, I. J.; Figdor, C. G. Multimodal imaging of nanovaccine carriers targeted to human dendritic cells. *Mol. Pharmaceutics* **2011**, *8* (2), 520−31.
(19) Blois, S.; Alba Soto, C. D.; Olmos, S.; Chuluyan, E.; Gentile, T.; Arck, P. C.; Margni, R. A. Therapy with dendritic cells influences the spontaneous resorption rate in the CBA/J x DBA/2J mouse model. *Am. J. Reprod. Immunol.* **2004**, *51* (1), 40−8.
(20) Bonetto, F.; Srinivas, M.; Weigelin, B.; Cruz, L. J.; Heerschap, A.; Friedl, P.; Figdor, C. G.; de Vries, I. J. A large-scale (19)F MRI-based cell migration assay to optimize cell therapy. *NMR Biomed.* **2012**, *25* (9), 1095−103.
(21) Friedl, P.; Brocker, E. B. Reconstructing Leukocyte Migration in 3D Extracellular Matrix by Time-Lapse Videomicroscopy and Computer-Assisted Tracking. *Methods Mol. Biol.* **2004**, *239*, 77−90.
(22) Vitiello, A.; Ishioka, G.; Grey, H. M.; Rose, R.; Farness, P.; LaFond, R.; Yuan, L.; Chisari, F. V.; Furze, J.; Bartholomeuz, R.; et al. Development of a lipopeptide-based therapeutic vaccine to treat chronic HBV infection. I. Induction of a primary cytotoxic T lymphocyte response in humans. *J. Clin. Invest.* **1995**, *95* (1), 341−9.
(23) Cruz, L. J.; Iglesias, E.; Aguilar, J. C.; Gonzalez, L. J.; Reyes, O.; Albericio, F.; Andreu, D. A comparative study of different presentation strategies for an HIV peptide immunogen. *Bioconjugate Chem.* **2004**, *15* (1), 112−20.
(24) Huang, S. H.; Liao, M. H.; Chen, D. H. Direct binding and characterization of lipase onto magnetic nanoparticles. *Biotechnol. Prog.* **2003**, *19* (3), 1095−100.
(25) Cruz, L. J.; Tacken, P. J.; Fokkink, R.; Joosten, B.; Stuart, M. C.; Albericio, F.; Torensma, R.; Figdor, C. G. Targeted PLGA nano- but not microparticles specifically deliver antigen to human dendritic cells via DC-SIGN in vitro. *J. Controlled Release 144*, (2), 118−26.
(26) Panyam, J.; Zhou, W. Z.; Prabha, S.; Sahoo, S. K.; Labhasetwar, V. Rapid endo-lysosomal escape of poly(DL-lactide-co-glycolide) nanoparticles: implications for drug and gene delivery. *FASEB J.* **2002**, *16* (10), 1217−26.
(27) Shen, H.; Ackerman, A. L.; Cody, V.; Giodini, A.; Hinson, E. R.; Cresswell, P.; Edelson, R. L.; Saltzman, W. M.; Hanlon, D. J. Enhanced and prolonged cross-presentation following endosomal escape of exogenous antigens encapsulated in biodegradable nanoparticles. *Immunology* **2006**, *117* (1), 78−88.
(28) Verdijk, P.; Aarntzen, E. H.; Lesterhuis, W. J.; Boullart, A. C.; Kok, E.; van Rossum, M. M.; Strijk, S.; Eijckeler, F.; Bonenkamp, J. J.; Jacobs, J. F.; Blokx, W.; Vankrieken, J. H.; Joosten, I.; Boerman, O. C.; Oyen, W. J.; Adema, G.; Punt, C. J.; Figdor, C. G.; de Vries, I. J. Limited amounts of dendritic cells migrate into the T-cell area of lymph nodes but have high immune activating potential in melanoma patients. *Clin. Cancer Res.* **2009**, *15* (7), 2531−40.
(29) Kim, D. H.; Martin, D. C. Sustained release of dexamethasone from hydrophilic matrices using PLGA nanoparticles for neural drug delivery. *Biomaterials* **2006**, *27* (15), 3031−7.
(30) de Chickera, S. N.; Snir, J.; Willert, C.; Rohani, R.; Foley, R.; Foster, P. J.; Dekaban, G. A. Labelling dendritic cells with SPIO has implications for their subsequent in vivo migration as assessed with cellular MRI. *Contrast Media Mol. Imaging* **2011**, *6* (4), 314−27.
(31) Cheong, C.; Matos, I.; Choi, J. H.; Dandamudi, D. B.; Shrestha, E.; Longhi, M. P.; Jeffrey, K. L.; Anthony, R. M.; Kluger, C.; Nchinda, G.; Koh, H.; Rodriguez, A.; Idoyaga, J.; Pack, M.; Velinzon, K.; Park, C. G.; Steinman, R. M. Microbial stimulation fully differentiates monocytes to DC-SIGN/CD209(+) dendritic cells for immune T cell areas. *Cell* **2010**, *143* (3), 416−29.
(32) Tacken, P. J.; Zeelenberg, I. S.; Cruz, L. J.; van Hout-Kuijer, M. A.; van de Glind, G.; Fokkink, R. G.; Lambeck, A. J.; Figdor, C. G. Targeted delivery of TLR ligands to human and mouse dendritic cells strongly enhances adjuvanticity. *Blood* **2011**, *118* (26), 6836−44.